Geophysical Prospecting EAGE EUROPEAN ASSOCIATION OF GEOSCIENTISTS & ENGINEERS

Geophysical Prospecting, 2009, **57**, 957–979 doi: 10.1111/j.1365-2478.2009.00789.x

Operator-oriented CRS interpolation

German Hoecht[1*], Patrice Ricarte[2], Steffen Bergler[3‡] and Evgeny Landa[1]

[1]*OPERA, Bâtiment IFR, rue Jules Ferry, 64000 Pau, France,* [2]*Institut Français du Pétrole (IFP), 1-4 avenue de Bois-Preau, 92852 Ruiel Malmaison Cedex, France, and* [3]*Shell International Exploration & Production, Kessler Park 1, 2288 GS Rijswijk, The Netherlands*

Received June 2008, revision accepted November 2008

ABSTRACT

In common-reflection-surface imaging the reflection arrival time field is parameterized by operators that are of higher dimension or order than in conventional methods. Using the common-reflection-surface approach locally in the unmigrated prestack data domain opens a potential for trace regularization and interpolation. In most data interpolation methods based on local coherency estimation, a single operator is designed for a target sample and the output amplitude is defined as a weighted average along the operator. This approach may fail in presence of interfering events or strong amplitude and phase variations. In this paper we introduce an alternative scheme in which there is no need for an operator to be defined at the target sample itself. Instead, the amplitude at a target sample is constructed from multiple operators estimated at different positions. In this case one operator may contribute to the construction of several target samples. Vice versa, a target sample might receive contributions from different operators. Operators are determined on a grid which can be sparser than the output grid. This allows to dramatically decrease the computational costs. In addition, the use of multiple operators for a single target sample stabilizes the interpolation results and implicitly allows several contributions in case of interfering events. Due to the considerable computational expense, common-reflection-surface interpolation is limited to work in subsets of the prestack data. We present the general workflow of a common-reflection-surface-based regularization/interpolation for 3D data volumes. This workflow has been applied to an OBC common-receiver volume and binned common-offset subsets of a 3D marine data set. The impact of a common-reflection-surface regularization is demonstrated by means of a subsequent time migration. In comparison to the time migrations of the original and DMO-interpolated data, the results show particular improvements in view of the continuity of reflections events. This gain is confirmed by an automatic picking of a horizon in the stacked time migrations.

INTRODUCTION

Different interpolation strategies have been investigated and used in the past: linear prediction error filtering (Spitz 1991), Fourier reconstruction (Sacchi and Ulrych 1996) or Radon transform (Trad 2003) are among the most popular ones. These techniques are based on the decomposition of the local wavefield in a transformed domain (Thorson and Claerbout 1985; Hugonnet and Canadas 1997; Kao 1997). After analysis and processing the inverse transformation restores the wavefield on the desired output grid. These methods use different assumptions and work in different data domains. However, they can suffer from sparse and irregular data geometries and

*E-mail: german.hoecht@univ-pau.fr
‡Formerly Geophysical Institute Karlsruhe, Germany

© 2009 European Association of Geoscientists & Engineers

require additional efforts to account for this problem (Xu *et al.* 2005).

In this paper we present an interpolation based on the common-reflection-surface (CRS) approach which uses attributes that describe the kinematics of the measured wavefield (Jäger *et al.* 2001; Zhang *et al.* 2001). These attributes represent parameters that are estimated from the data by means of a second-order approximation of the reflection traveltimes in the time domain. The CRS technique is mostly known for its application to produce a zero-offset (ZO) stack (Jäger *et al.* 2001). Here, the estimated parameters can be subsequently utilized for a tomographic velocity model inversion (Duveneck 2004; Della Moretta *et al.* 2006). For the ZO CRS application the traveltimes of reflection events are approximated in the vicinity of a ZO reflection associated with a normal ray. A more general approach is given by the common-offset (CO) CRS (Zhang *et al.* 2001), which allows to approximate traveltimes of reflection events in the vicinity of arbitrary central rays and, thus, at arbitrary offsets. The CRS theory can in fact easily be extended to any dimension and acquisition geometry when interpreting the CRS operator as a local second-order traveltime approximation of reflection events. In this paper we use this local description for the purpose of trace interpolation. In addition to the published CRS interpolation scheme (Hoecht *et al.* 2004; Hoecht and Ricarte 2006a), we introduce a so-called operator-oriented technique which is particularly suited for a CRS-type imaging scheme (Hoecht and Ricarte 2006b). The aim of this approach is to avoid the definition of an operator at an output sample as required by a standard scheme to which we refer to as target-oriented scheme. The new approach makes use of the redundancy of CRS operators in the data space and implicitly allows to define several operators per target sample.

We present the general workflow and the implementation of a CRS interpolation and give a detailed introduction to the operator-oriented scheme. This new technique is compared to the target-oriented scheme with respect to theoretical and practical aspects. The operator-oriented scheme has been applied in order to regularize an ocean bottom cable (OBC) common-receiver volume and common-offset subsets of a 3D marine data set. We refer to these subsets as common-offset classes. They are built using a binning in offset so that the offset variations within a class is limited by a chosen bin size in offset. In the latter application, we focus on the impact of the regularization on the quality of subsequent post-processing steps. For that purpose, we compare time-migrated common-offset classes of the original and regularized data and benchmark the results with a dip moveout (DMO) regularization.

BASICS

CRS-based interpolation works in the time domain and is based on the estimation of local kinematic attributes of the wavefield. It makes use of a local second-order traveltime approximation and can be applied to any data where locally coherent events are present. Although theoretically possible for any data dimension, we restrict ourselves to a 3D data space in the following.

Figure 1 shows some data traces (black) and a target trace (green) which is to be generated in a 3D data cube. The general idea of the interpolation scheme is to extract local information from the existing measured traces and to use this information to construct a new, interpolated trace.

The operator for a sample $\hat{t}$ of the target trace located at $(\hat{x}, \hat{y})$ is given by the following local parabolic second-order

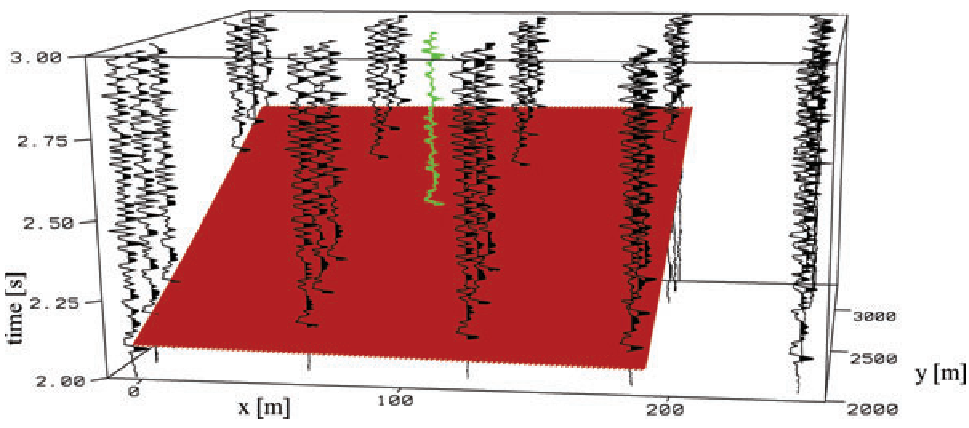

Figure 1 Interpolation in a 3D data space (t, x, y): the data traces are illustrated in black, the target trace to be interpolated is shown in green. The operator given by equation (1) for a sample of the target trace is shown in dark red.

traveltime approximation:

$$\Delta t = t(\Delta x, \Delta y) - \hat{t} = b_0\,\Delta x + b_1\,\Delta y + a_{00}\,\Delta x^2 + a_{01}\,\Delta x\,\Delta y + a_{11}\,\Delta y^2\,. \tag{1}$$

Here, the traveltime difference $\Delta\ t$ describes the moveout of a reflection event relative to the investigated sample $\hat{t}$ of the target trace. The variables $\Delta x = x - \hat{x}$ and $\Delta y = y - \hat{y}$ denote the positions $(x,\ y)$ of the data traces relative to the target trace located at $(\hat{x}, \hat{y})$. The parameters $b_0,\ b_1$ are the first-order, $a_{00},\ a_{01},\ a_{11}$ are the second-order spatial traveltime derivatives, respectively. For 2D acquisition, these parameters can be related to wavefront orientations and curvatures of different observation configurations (common-shot, common-receiver, and a hypothetical common-midpoint experiment, see Zhang *et al.* (2001)).

An operator given by equation (1) is involved twice in the interpolation procedure: firstly, we need to estimate it from the data, and secondly, we perform a (weighted) stack along it to simulate the amplitude at a sample of the target trace. However, to reduce the computational cost it is essential to estimate the operators on a coarse grid. Therefore, we define three different grids in the data space: the data grid, the parameter grid and the target grid. These grids are intended to define the positions of different types of traces. The (irregular) data grid is defined by the locations of the actually acquired data traces. The parameter grid defines the location of parameter traces where the operators are estimated for each sample. The target grid is a chosen grid and carries the target traces where the wavefield needs to be simulated. We will refer to the samples of the different data traces, parameter traces, and target traces as data samples, parameter samples, and target samples.

After the estimation of the operators on the parameter grid an operator is defined by a parameter set (b_0, b_1, a_{00}, a_{01}, a_{11}) at a parameter sample $\hat{t}$. For the final interpolation it is necessary to define the operators at the target traces. For that purpose, existing schemes interpolate the parameters from the parameter traces to the target traces. We will refer to this technique as target-oriented (TO) scheme and introduce an alternative operator-oriented (OO) scheme which, among other things, avoids the drawbacks of a parameter interpolation. In the following we discuss the different steps involved in the parameter estimation and interpolation. Afterwards, we present and compare the TO and OO schemes.

IMPLEMENTATION

Estimation of parameters

For the kinematic description of locally coherent events by means of equation (1) we create parameter traces at chosen positions. The five parameters that define an operator have to be estimated for each sample of these parameter traces. However, the ideal solution of a simultaneous five-parameter estimation is computationally too expensive. There are different ways to determine the five parameters of equation (1) separately. One way is to firstly neglect the second-order terms and to start with a linear (plane) operator (i.e., to reduce the operator in the order) and to estimate the second-order terms afterwards. Another approach is to limit the operator in dimensions and to estimate the parameters in various subsets. Both strategies have their advantages and disadvantages. A limitation in the order does not require subsets and treats all dimensions

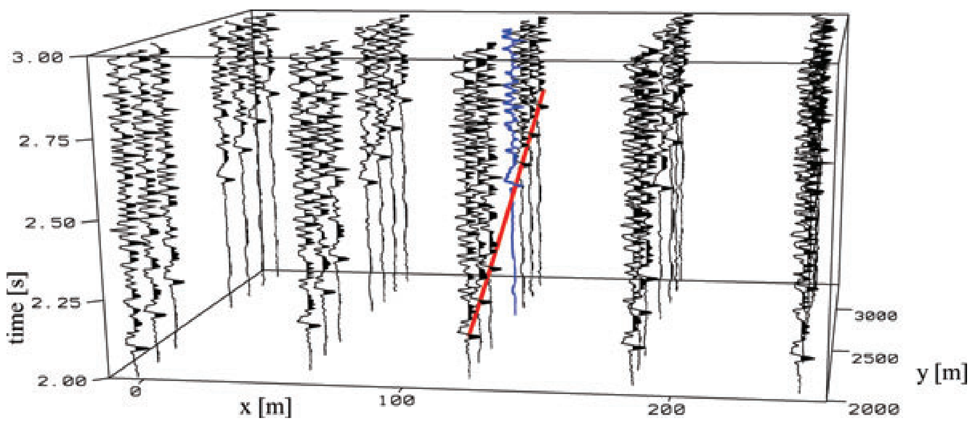

Figure 2 Estimation of the parameters b_1 and a_{11} for a sample of a parameter trace (blue) within a bin in x-direction. The estimated operator is shown in red.

© 2009 European Association of Geoscientists & Engineers,

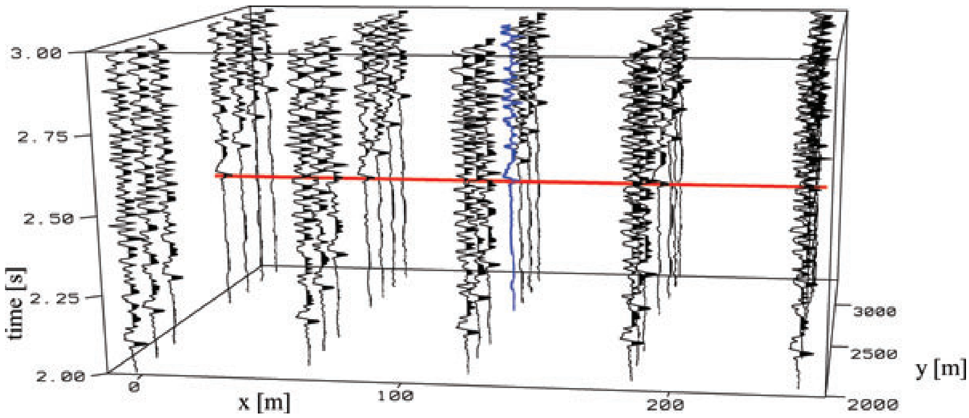

Figure 3 Estimation of the parameters b_0 and a_{00} for a sample of a parameter trace (blue) within a bin in y-direction. The estimated operator is shown in red.

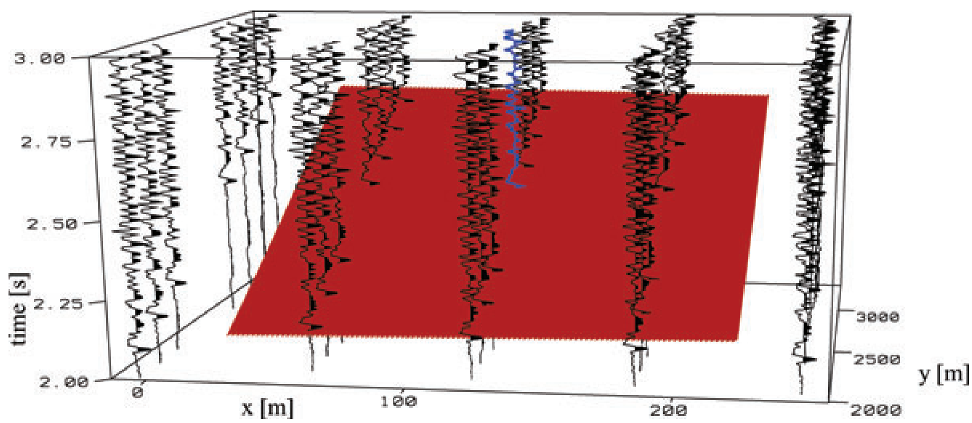

Figure 4 Estimation of the parameter a_{01} for a sample of a parameter trace (blue) within the data volume. The final operator is shown in red.

simultaneously but is more susceptible to aliasing in one of the dimensions. Constraining the dimensions keeps the order of approximation but has the disadvantage that data subsets are considered independently. Both approaches decrease the stability and continuity of the parameters. The choice among these approaches remains a compromise and will in general depend on the data geometry. Our choice here is to maintain the second-order terms and to estimate the parameters using different subsets of the data space. Due to the data irregularities and the parameter estimation in subsets, the data are binned in both spatial dimensions of the data volume. Note that this binning does not change the trace coordinates but serves to group the data traces. Within the binned data grid we choose the parameter grid which is in general coarser than the data grid. Figure 2 shows the position of a parameter trace (blue) in the data volume.

Step 1: two-parameter estimation in first bin direction

In the first step we fix one of the two spatial coordinates. Setting $x = \hat{x}$ we consider a (binned) 2D section of the data in which the surface described by equation (1) reduces to a curve:

$$t(\Delta y) = \hat{t} + b_1\,\Delta y + a_{11}\,\Delta y^2\,. \tag{2}$$

Here, Δy denotes the relative coordinates of the data traces to a parameter trace within the 2D section. The irregularities in the orthogonal direction Δx of the involved data traces are neglected in equation (2). However, this error is constrained by the bin spacing in x-direction. The operator of equation (2) serves to describe the kinematics of the reflection events and has to be estimated from the data for each time sample $\hat{t}$ of the parameter trace. This is done by simultaneous variation of

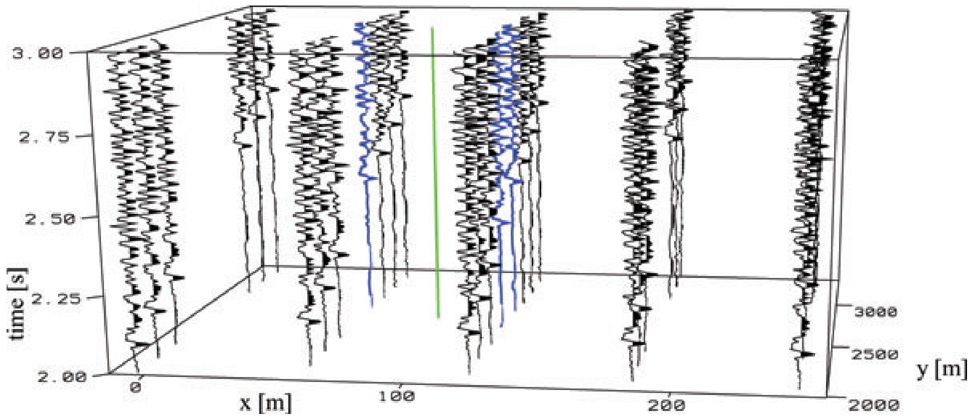

Figure 5 Position of a target trace (green) and three enclosing parameter traces (blue). The parameters allow to construct the operators at the parameter traces but these are required at the target trace.

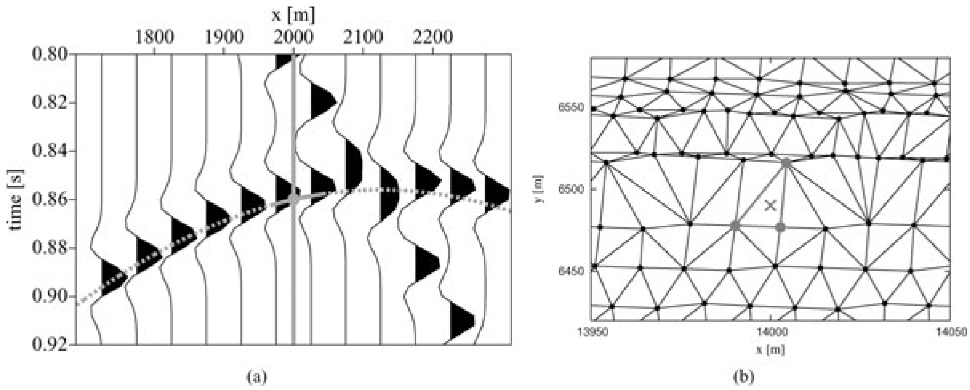

Figure 6 a) operator (dashed curve) for a sample (gray dot) of the target trace (gray). For CRS interpolation only the amplitudes from the enclosing traces are involved. For the displayed 2D case the amplitudes along the solid part of the operator are used. b) triangulation of the data traces in case of a 3D geometry. The positions of the data traces are displayed by black dots, the position of the target trace is illustrated by a gray cross. For interpolation, the amplitudes from the three traces of the triangle (gray) enclosing the target trace are involved.

the parameters (b_1, a_{11}) and coherency analysis along the operator for each parameter set (b_1, a_{11}). The operator yielding the highest coherency is selected and defines the parameter set (b_1, a_{11}) for the respective time sample $\hat{t}$ (Fig. 2).

Step 2: two-parameter estimation in second bin direction

Analogously to the first step, we perform a simultaneous two-parameter estimation in the second spatial bin direction (Fig. 3). Therefore, we set $y = \hat{y}$ which reduces equation (1) to the curve

$$t(\Delta x) = \hat{t} + b_0\,\Delta x + a_{00}\,\Delta x^2\,. \tag{3}$$

Again, the parameters b_0 and a_{00} are determined for each sample of the parameter trace. Here, we neglect the spatial deviation Δy of the involved data traces. Note that step one and two are independent of each other and, thus, permutable.

Step 3: one-parameter estimation along surface

Once the parameters b_0, b_1, a_{00}, and a_{11} are available for a sample $\hat{t}$ of a parameter trace the mixed second-order traveltime derivative a_{01} can be estimated using the surface given by equation (1). In this one-parameter estimation we consider the data traces within a two-dimensional aperture. Here, the true data coordinates (without any binning restrictions) are employed. Figure 4 illustrates the involved operator for a sample of a parameter trace.

Interpolation

Because the parameter grid and the target grid can be different, we have to define operators at the target traces based on the operators estimated at the parameter traces. Figure 5 illustrates a possible configuration of a target trace, the data traces and three parameter traces.

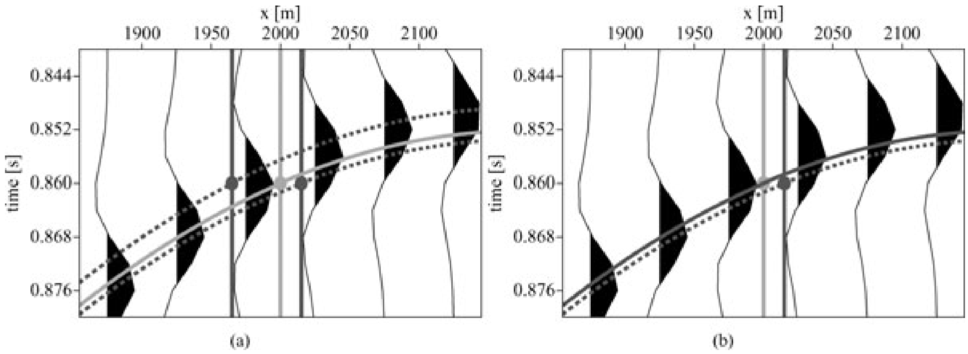

Figure 7 Illustration of the TO and OO schemes. a) TO scheme: the operator (light gray) is constructed at the target sample (light gray dot) after interpolation of the parameters from the samples (dark gray dots) of the enclosing parameter traces (dark gray). b) OO scheme: the operator is constructed at a sample of a parameter trace and intersects the target trace near a target sample (light gray dot). To match the target sample the operator is shifted in time (dark gray curve).

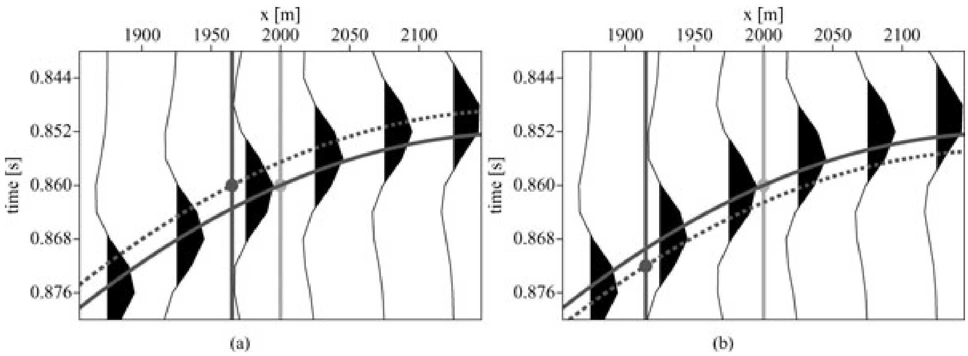

Figure 8 OO scheme: contributions to the same target sample from different parameter traces. In both figures, the operator (dashed gray curve) is constructed at a parameter sample (dark gray dot). The time-shifted operator for a target sample (light gray dot) is shown as solid gray curve.

Operator construction

In order to define the operators at a target trace we distinguish between two schemes: a TO scheme and an OO scheme. For the TO scheme the parameters are interpolated to the target trace. Subsequently, these interpolated parameters can be employed to construct the operator at the target sample according to equation (1). This results in one single operator per target sample.

In contrast, in the OO scheme the operator is directly constructed at a sample of the parameter trace. The intersection point of the operator with a target trace defines an operator for the respective sample of the target trace. In this scheme several operators can contribute to the same target sample.

Trace interpolation

Let us assume that an operator is available at a target sample. For the actual interpolation of the seismic, the amplitudes of the data traces are summed along the operator and assigned to the sample of a target trace as illustrated in Fig. 1. However, we only involve data traces in the neighborhood of a target trace to preserve the local character of the data. In addition, the amplitude contributions are weighted according to their distances to the target traces. Figure 6(a) illustrates the interpolation scheme for the 2D case. The target trace is located between two data traces and shown together with the operator for a target sample. For the interpolation we use only the two neighboring data samples defined by the operator. The 3D case requires a more complex handling. Here, we involve a triangulation of the data geometry to determine three data traces that enclose the target trace (Fig. 6b).

This principle is applied in the TO as well as in the OO scheme: a contributing operator provides a weighted summation of amplitudes from the data traces that enclose the target trace. Because several operators can contribute to a target sample in the OO scheme, the sum of the individual operator contributions is divided by the number of contributing operators.

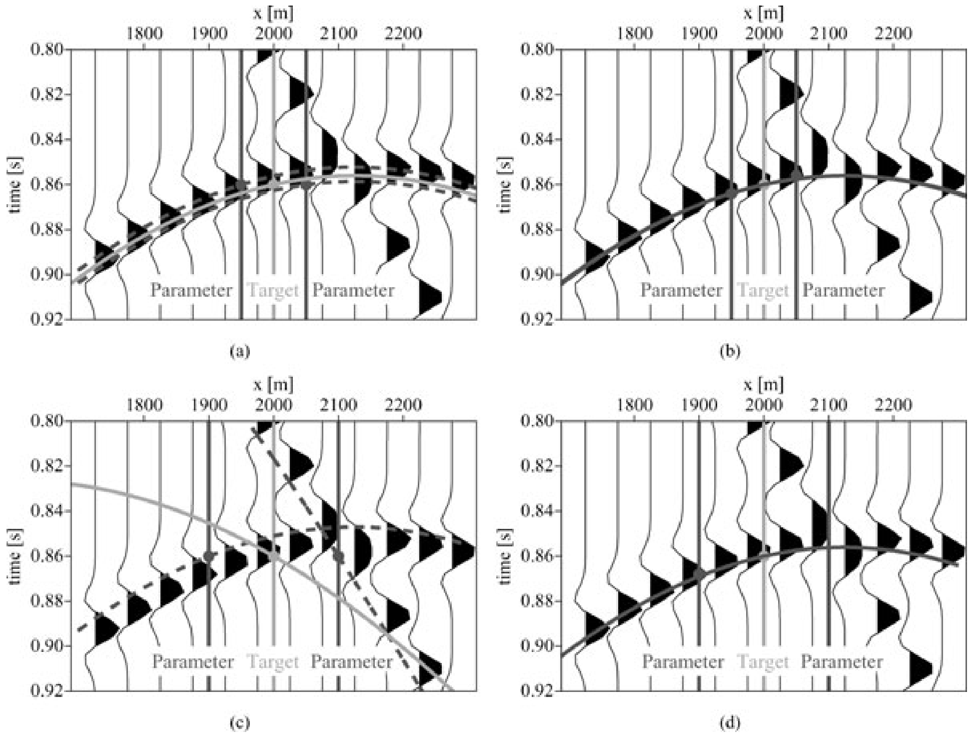

Figure 9 Comparison of the TO scheme (left) and the OO scheme (right). a-b) for a single reflection event and a dense parameter grid, both schemes provide similar operators (solid curves) at the target sample (light gray dot). c-d) in case of a coarse parameter grid, an interfering event may easily provoke inconsistent parameter interpolation in the TO scheme, whereas the OO scheme still provides a correct operator at the target sample. Note that for clarity, the operators estimated at the parameter samples (dashed gray curves) are only shown for the TO scheme. All contributing operators are displayed for the OO scheme: in case of Fig. (b), where both parameter traces contribute, the operators visually match in the shown range.

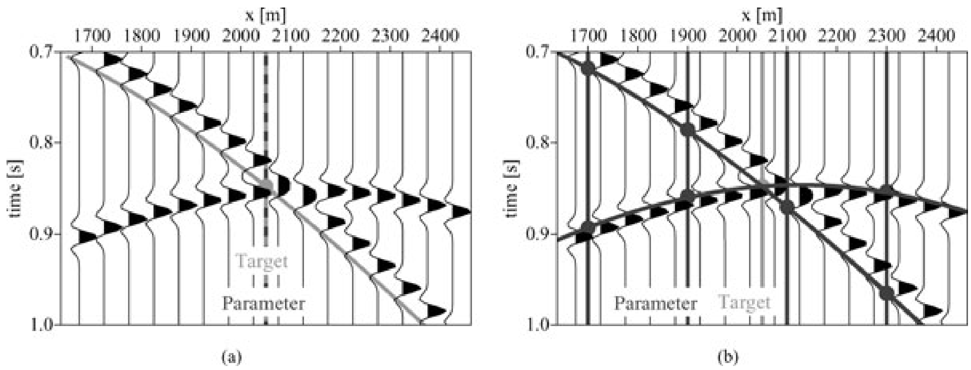

Figure 10 Conflicting dip situation: a) the TO scheme uses only contributions from a single operator (gray curve) and, thereby, from one reflection event whereas b) the OO scheme collects contributions from both reflection events. Again, all contributing operators in the OO scheme are displayed. They visually match perfectly along the two events.

TARGET- AND OPERATOR-ORIENTED SCHEMES

As described above, we distinguish between a parameter grid and a target grid. The operators (equation (1)) estimated for each sample of the parameter traces have now to be defined for samples of the target traces. In the following we compare two schemes which differ in the way the operators from the parameter traces are assigned to the target traces. We firstly describe the commonly used TO scheme and afterwards introduce the OO scheme. For their explanation it is sufficient to consider the interpolation within a 2D seismic gather.

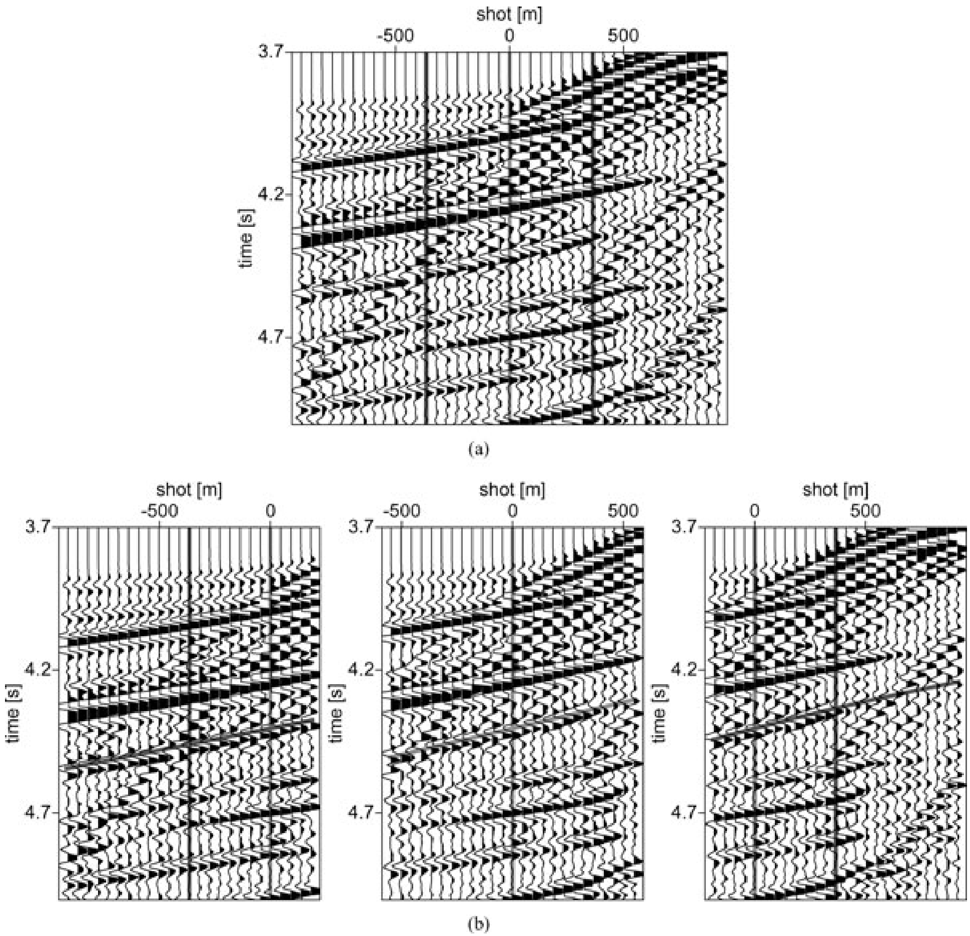

Figure 11 Sigsbee data: a) subset of the common-offset section for offset 1212 m with three parameter traces illustrated in gray. The target trace coincides with the central parameter trace depicted in light gray. b) related search ranges for the three parameter traces: the operators of the different parameter traces are estimated in different overlapping subsets. One operator (curve) per parameter trace is shown exemplarily for a sample.

Figure 7 shows a subset of such a gather together with the positions of a target trace and its enclosing parameter traces.

Target-oriented scheme

Figure 7(a) illustrates the TO scheme. The operators defined at the parameter traces are illustrated for two samples of the parameter traces. In the TO scheme we interpolate the parameters from the neighboring parameter traces to the target trace and thereby construct a parameter trace at the target position. The interpolation of parameters is done by a distance-weighted linear interpolation of the enclosing parameter traces. The resulting parameters define a unique operator for each sample of the target trace as illustrated for one target sample in the figure.

This principle analogously applies to a 3D data volume (t, x, y) where we involve the three parameter traces enclosing the target trace for the parameter interpolation. Note that in case of coincident parameter traces and target traces, no interpolation of the parameters is required.

Operator-oriented scheme

In contrast to the TO scheme, the OO scheme does not involve the interpolation of parameters but here we directly construct the operator at a sample of a parameter trace. Figure 7(b) shows a sample of a parameter trace and the corresponding operator. To make use of this operator for a target trace, we firstly compute its intersection point with the target trace. Subsequently, the operator is shifted in time from the intersection point to a neighboring target sample (Fig. 7b).

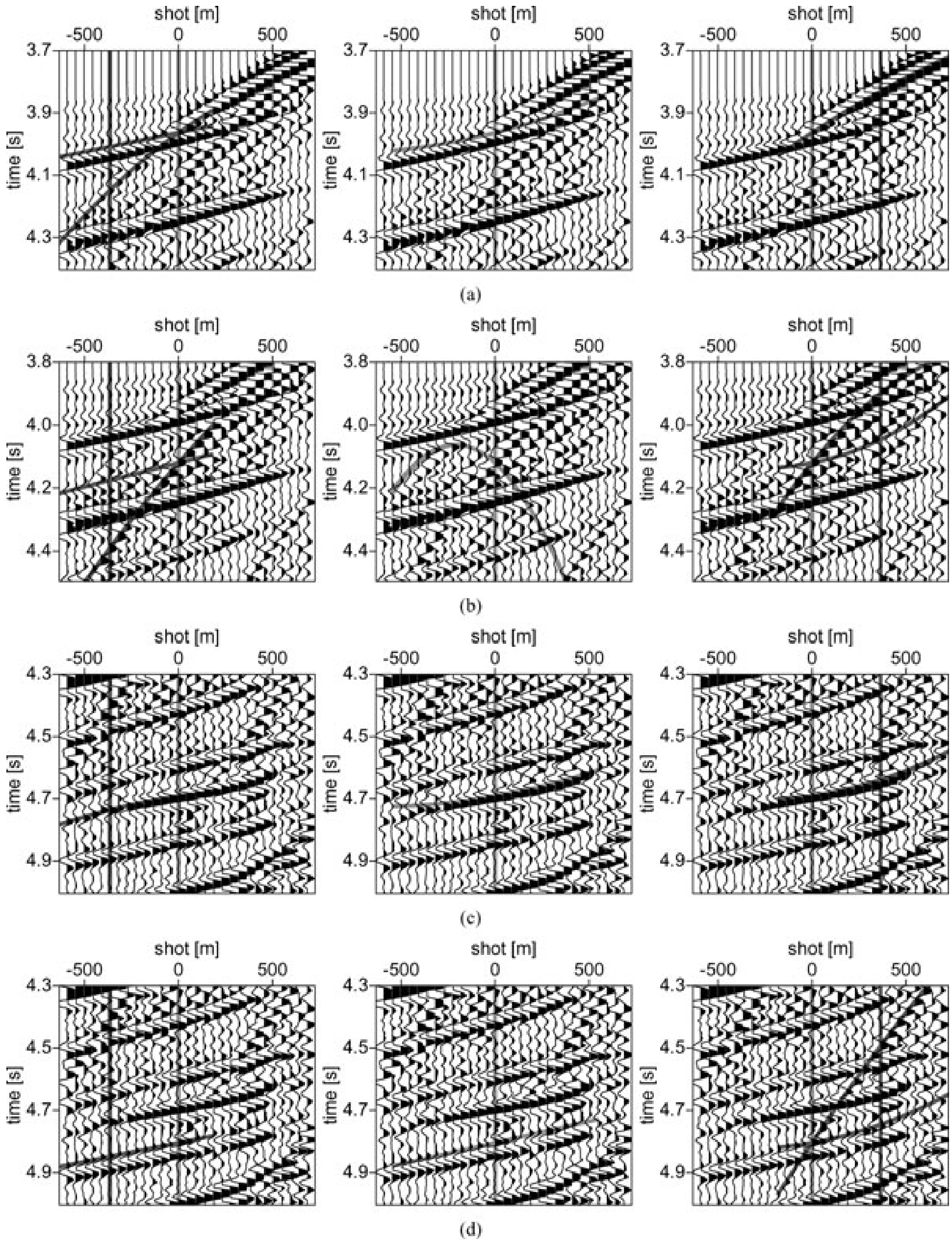

Figure 12 Sigsbee data: contributing operators for different target samples in a common-offset section for offset 1212 m. Each row of pictures investigates a different target sample found at the intersection of the operators with the target trace (light gray). The TO scheme is confined to the operators from the coincident parameter trace (middle column), whereas the OO scheme involves all operators.

In the OO scheme each sample of a parameter defines an operator and individually contributes to a target trace. Therefore, we can involve other parameter traces in addition to the parameter traces enclosing the target trace. Figure 8 shows the contributions from such additional parameter traces to the same target sample. Although the operators can stem from more distant parameter traces, the amplitudes used for the actual interpolation of the target trace are always taken from its enclosing data traces.

The OO scheme can be applied in a similar manner for data of higher dimension. In case of a 3D data volume (t, x, y) the operators form surfaces as given by equation (1) so that a target trace can receive contributions from parameter traces located in any spatial direction.

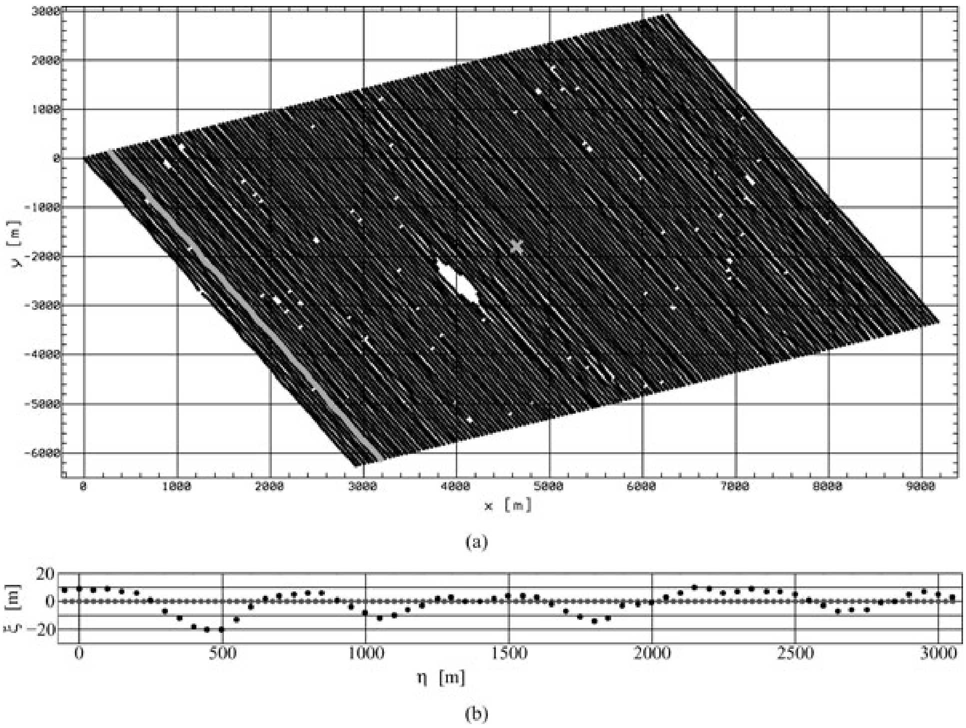

Figure 13 OBC data: a) geometry of the 3D common receiver gather. The gray cross represents the receiver position, the shot positions are denoted by black dots. The gray dots indicates the selected line displayed in the bottom; b) irregularities of the actual shots (black) and the positions of the interpolated shots (gray) along the selected line.

In the following, we discuss the differences between the two schemes and illustrate the impact of using more distant parameter traces in case of a complex wavefield as present in the Sigsbee 2A data set from the SMAART consortium.

Comparison of the TO scheme and the OO scheme

To point out the major differences between the two schemes we analyze the operators for a target sample within a seismic section that contains two crossing events (Figs 9 and 10).

Figures 9(a) and 9(c) illustrate the TO scheme where the parameters are interpolated to the target sample. For the time associated with the target sample the operators attached to the parameter traces are displayed: in Fig. 9(a) the parameter traces are located close to the target trace and provide similar operators. Therefore, a parameter interpolation to the target sample yields an operator that fits the reflection event. In Fig. 9(c) we increase the distance between parameter traces and the target trace. While the parameter trace on the left would provide a reasonable operator for the target sample, the parameter trace on the right defines an operator that follows the second event. The discrepancy between both operators results in an inappropriate operator at the target sample. This example illustrates the weakness of the parameter interpolation required for the TO scheme.

The OO scheme only allows contributions from operators that intersect the target trace close to the target sample. In case of a dense parameter grid as illustrated in Fig. 9(b), both parameter traces contribute to the target trace and provide almost the same operator at the target sample. In case of a sparse grid as illustrated in Fig. 9(d), only an operator from a sample of the left parameter trace contributes to the target sample. The right parameter trace does not provide any operator intersecting the target trace close to the target sample. Although the number of contributing operators reduces in case of a coarser grid, a suited operator is still available through the contribution from the left parameter trace.

Figures 10 shows a conflicting dip situation. For the TO approach shown in Fig. 10(a) we use a coincident parameter and target trace. Here, the single operator for a target sample follows the reflection event with the higher coherency. Figure 10(b) shows the operators from different parameter traces that contribute to the target sample in the OO scheme. Here, the operators that contribute to the target sample cover both reflection events. However, the number of operators from the two events can differ providing a biased result.

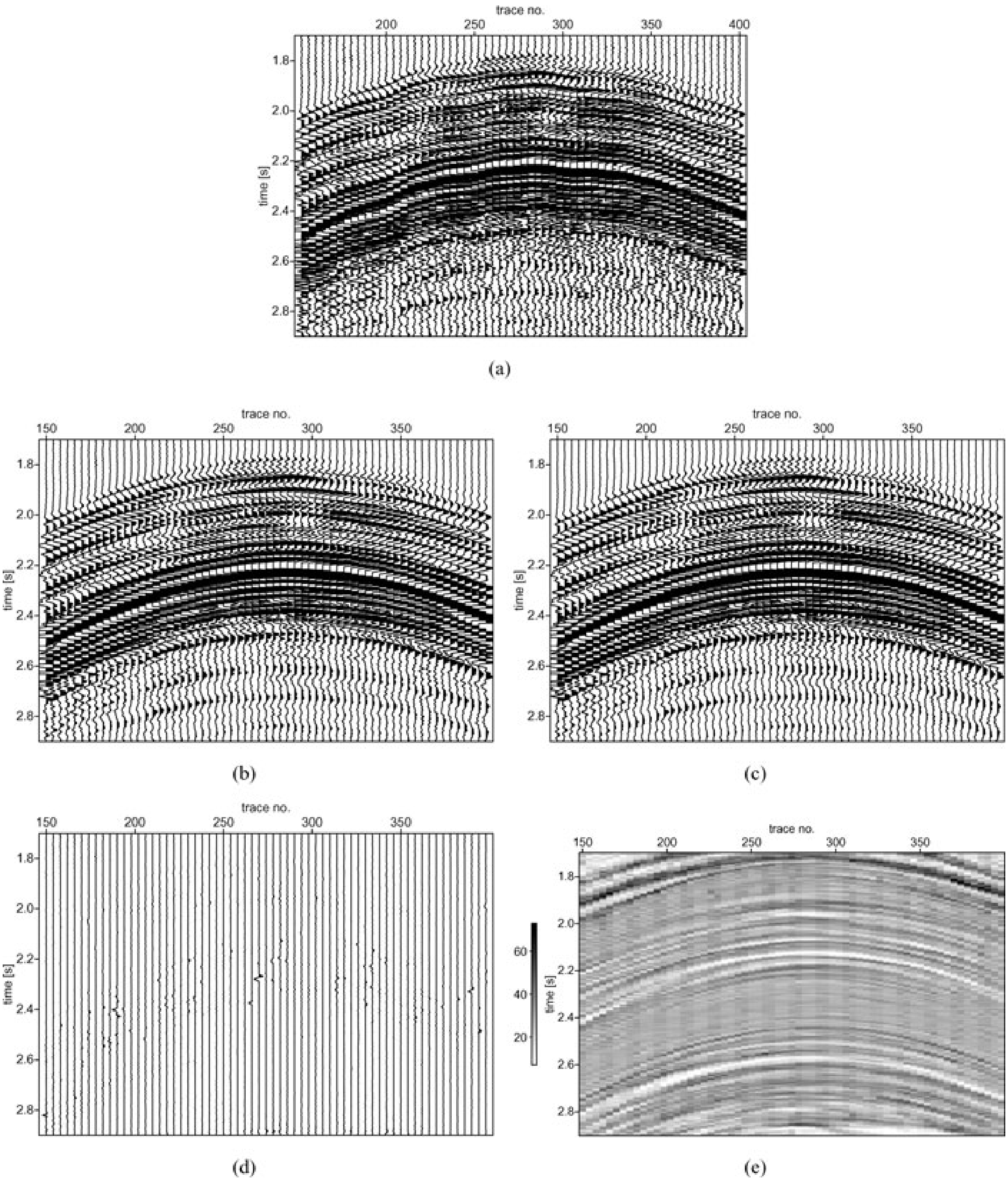

Figure 14 OBC data: data and interpolation results between existing traces: a) original data, b) TO interpolation, c) OO interpolation, d) difference of both interpolation results, e) OO interpolation: number of contributing operators per target sample.

Operators for a synthetic data example

Let us illustrate the impact of the OO scheme in case of complex synthetic data. Figure 11(a) shows a subset of a common-offset section from the Sigsbee 2A data set. Within this section we place three parameter traces one of which coincides with the target trace. For the estimation of the operators at the parameter traces we choose a symmetric aperture centered at the respective parameter trace. Accordingly, the three parameter traces use different data traces for the estimation of the parameters as shown in Fig. 11(b). For the analysis of the whole section it is reasonable to use overlapping apertures. It is important to note that the target trace is located within the respective aperture of each of the three parameter traces.

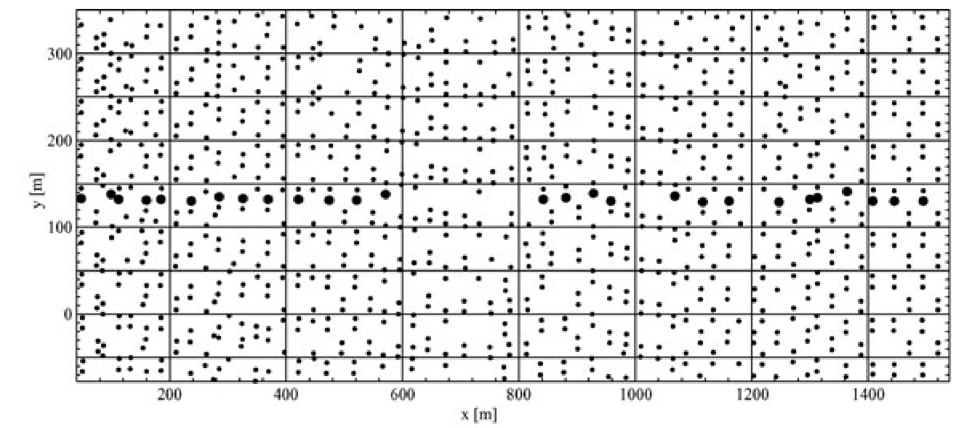

(a)

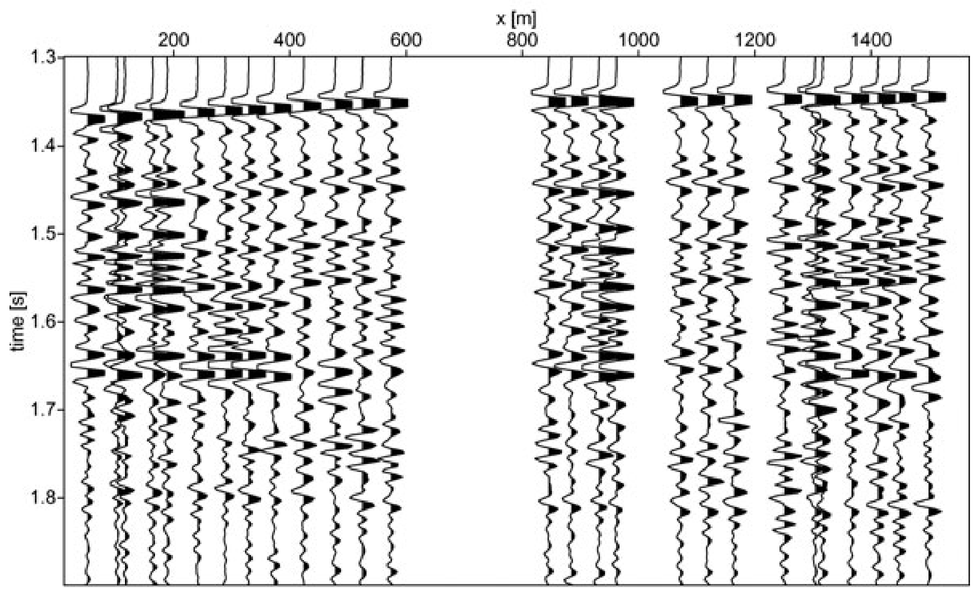

(b)

Figure 15 Marine data: a) midpoint geometry of the chosen offset class; b) section extracted along the line indicated by the bold dots in (a).

The TO scheme for the center target trace uses only the data subset shown in the middle of Fig. 11(b). In contrast, the OO scheme makes use of all three subsets, thus, offering different views to the target trace.

Let us now consider the effect of the different apertures for a chosen target trace by investigating the operators for some samples of this trace. Figure 12 shows the operators for four selected target samples. In the TO scheme, it is evident that the coincident target/parameter trace shown in the middle column of Fig. 12 yields only one operator per target sample. Additionally using the neighboring parameter traces in the OO scheme, we observe additional contributions to the target samples as shown in the left and right columns of Fig. 12. These operators may either follow the same locally coherent event as the operator attached to the central parameter trace like in Fig. 12(c), or they may provide contributions from other coherent events as shown in Fig. 12(a). In some cases these additional operators can hardly be identified at the target sample itself as for the steeply dipping event in Fig. 12(d) right. Figure 12(b) shows a situation where the operator estimated at the target trace does not follow an actual reflection event and, thus, causes an unwanted contribution to the target sample. The contributions from the enclosing parameter traces reduce its impact on the result.

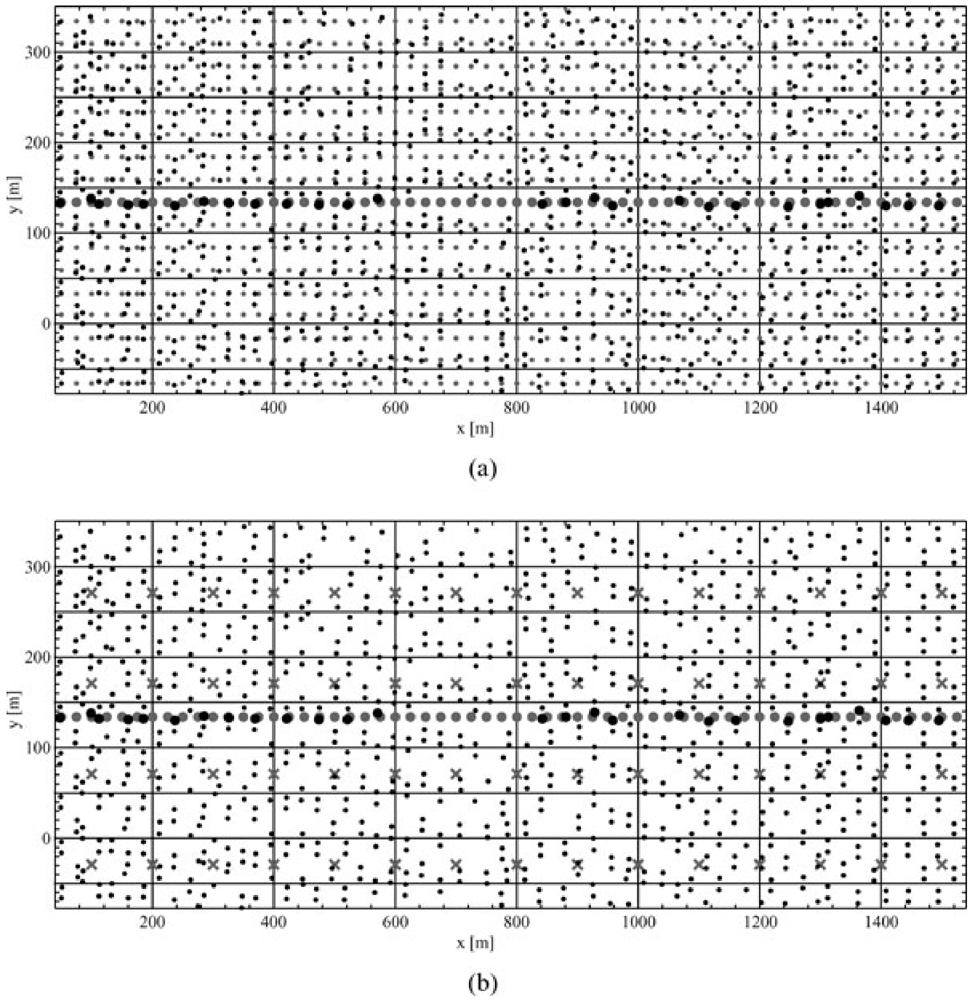

Figure 16 Marine data: midpoint geometries of a) the coincident target and TO parameter grid (gray dots) and b) the OO parameter grid (gray crosses). The original trace locations are represented by black dots, the selected line is depicted by bold black dots (irregular) and the corresponding positions of target traces (bold gray dots).

Summary

Due to the interpolation of parameters in the TO scheme to construct the operator at the target trace, this scheme requires a dense parameter grid. This restriction is considerably eased in the OO scheme where the operators are directly constructed at the parameter samples and are used independently. A coarse parameter grid is especially attractive in view of the computation time.

In general, one operator per target sample is involved in the TO scheme and all information relies on the accuracy of this operator. The OO scheme comprises the information of several operators and is based on constructive contributions from different parameter traces. Although this may have a smoothing effect, it stabilizes the interpolation result. Theoretically, we may find situations where no operators contribute to a target sample in the OO scheme. However, such circumstances are not expected along coherent events.

Both schemes do not handle conflicting dips situations properly. A 'proper' handling of conflicting dip situations requires to identify the different events in terms of kinematics and waveform. For the TO scheme, multiple operators would have to be estimated for this purpose. This involves more computational time and a sophisticated separation of the reflection events based on non-trivial rules that define signal, noise, and resolution. In the OO scheme multiple operators for a target sample are implicitly provided. However, because we do not select among the contributing operators the contributions may be unbalanced.

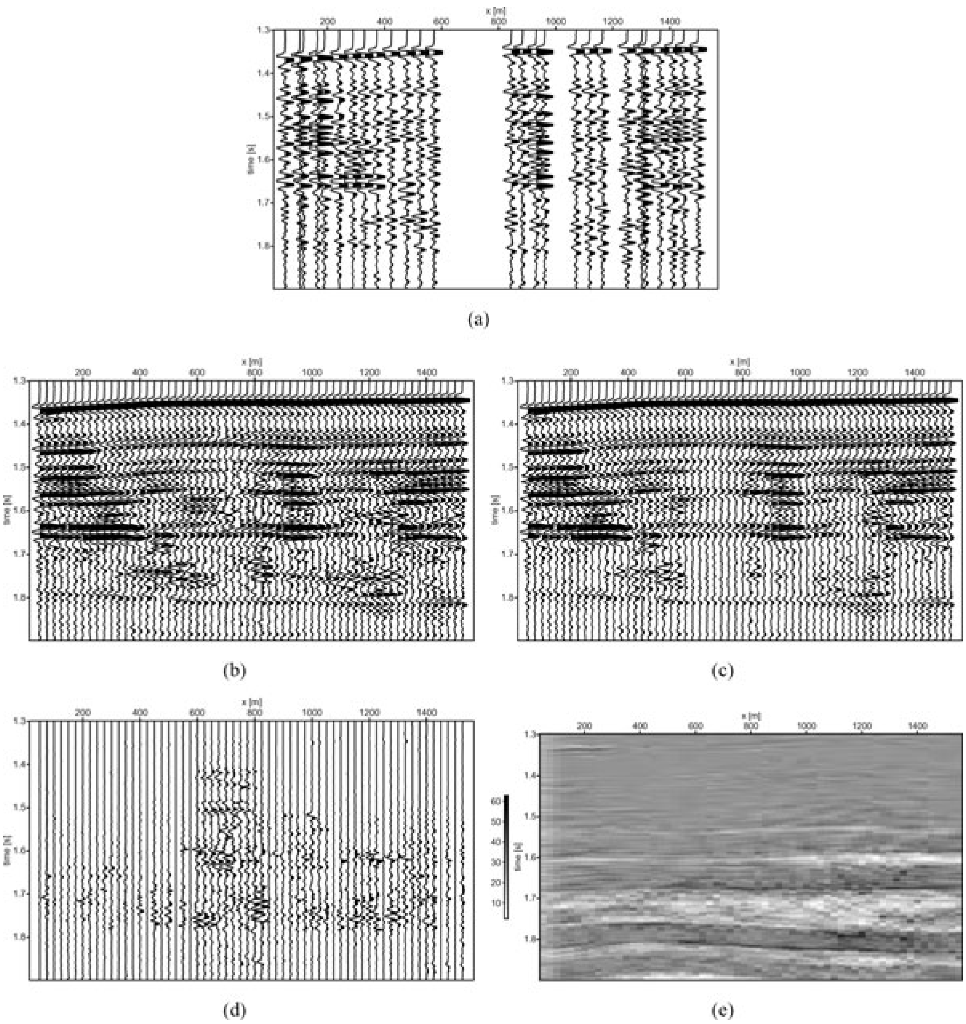

Figure 17 Marine data: data and interpolation results: a) original data, b) TO interpolation, c) OO interpolation, d) difference of both interpolation results. e) OO interpolation: number of contributing operators per target sample.

APPLICATION

Two major items are addressed here. Firstly, we want to demonstrate the effect of the OO scheme in practice. For this purpose, we compare the results with those obtained with the TO scheme for real data. Secondly, we investigate an application of the OO scheme with subsequent post-processing. In the latter application, we focus on the impact of a regularization on time migration and compare the results to a standard DMO regularization.

Comparisons of the TO and OO schemes for interpolation

For comparison of the two methods, we applied the TO and the OO CRS-based interpolation schemes to two data sets: a common-receiver gather extracted from a 3D OBC data set and a common-offset class extracted from a marine 3D single-azimuth data set. Both data sets are irregular and represent 3D data volumes. Our aim was to regularize and interpolate these data.

Interpolation of a 3D OBC common-receiver gather

Figure 13(a) shows the geometry of a 3D OBC common-receiver gather. In the following we will investigate a selected line which provides an irregular trace spacing in inline and crossline direction (Fig. 13b). The average trace spacing of the data is 50 m in both inline and crossline direction. The target was to regularize and interpolate the data to a

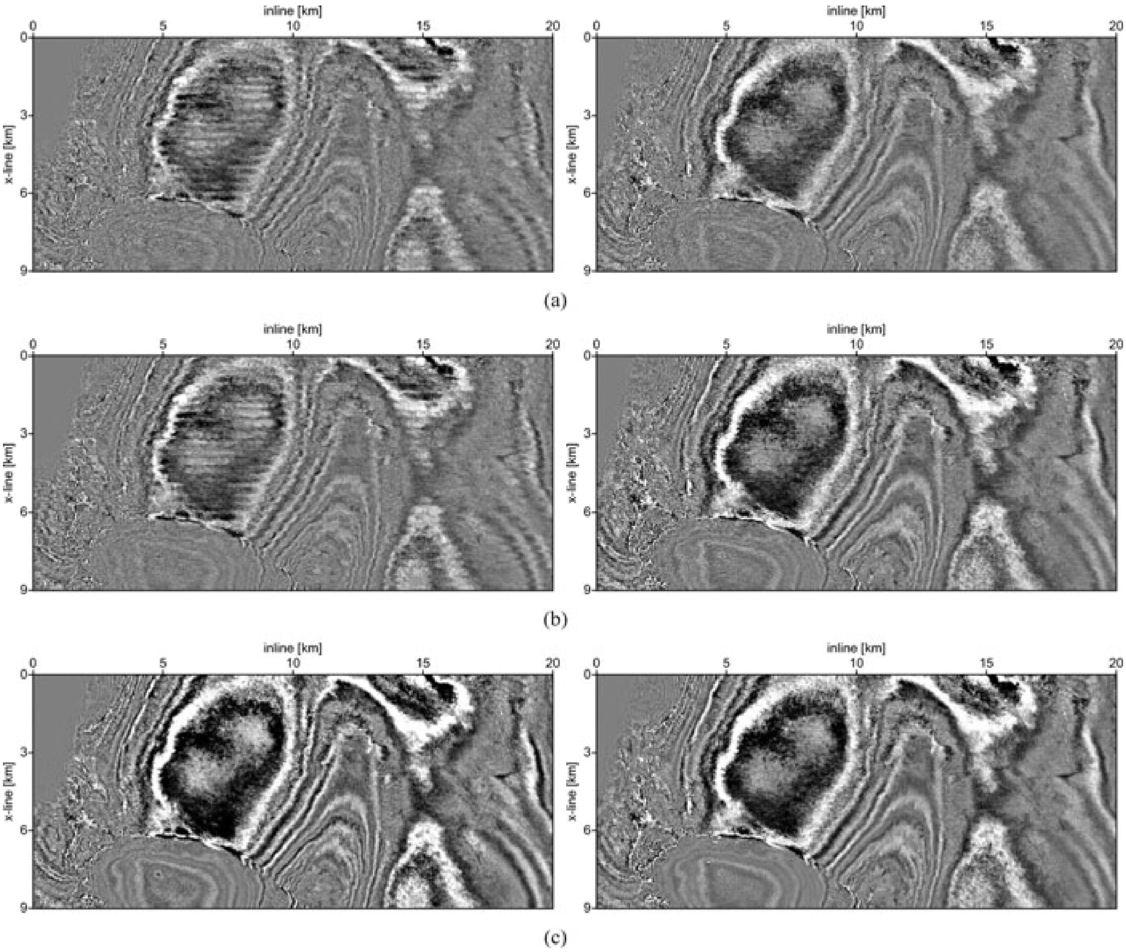

Figure 18 Marine data: time slices at 2.2 s of the two time-migrated common-offset classes 400 m (left) and 1500 m (right): a) original data; b) DMO-interpolated data; c) CRS-interpolated data.

regular trace spacing of 25 m × 25 m. For the TO interpolation a dense parameter grid of 50 m × 50 m has been chosen. For the OO interpolation the parameter grid was set to 200 m × 200m, which reduces the computational expense for the parameter estimation by a factor of 16.

Figure 14 shows the original data traces and the interpolation results. For the latter, we display only traces that are located in between the average data grid. As one can observe, the results of the TO interpolation (Fig. 14b) and the OO interpolation (Fig. 14c) are almost identical. This is confirmed by the difference section shown in Fig. 14(d). This example is well defined for the TO scheme because there are no large gaps and no crossing events, so that we do not expect any improvements with the OO scheme. However, it confirms the reliability and stability of the OO scheme. Although we use a coarser parameter grid and several operators per target sample (Fig. 14e) we obtain virtually the same result.

Interpolation of a 3D common-offset class

In this example we investigate the two schemes of CRS-based interpolation on a 3D single-azimuth common offset class. Figure 15(a) shows the midpoint geometry of the common-offset class with an offset range of 1450–1499 m. Figure 15(b) illustrates a selected line of this class. The trace spacing reflects the inline irregularities.

Figure 16 shows the midpoint geometries of the target grid (25 m × 25 m) that coincides with the TO parameter grid, and of the coarse OO parameter grid (100 m × 100 m). The OO parameter grid is defined by every fourth parameter trace of the TO grid in each direction, again reducing the computational cost by a factor of 16. For the parameter estimation, the data has been binned to a 25 m × 12.5 m grid.

Figure 17 shows the original data and the interpolation results. We observe again similar results from the TO scheme

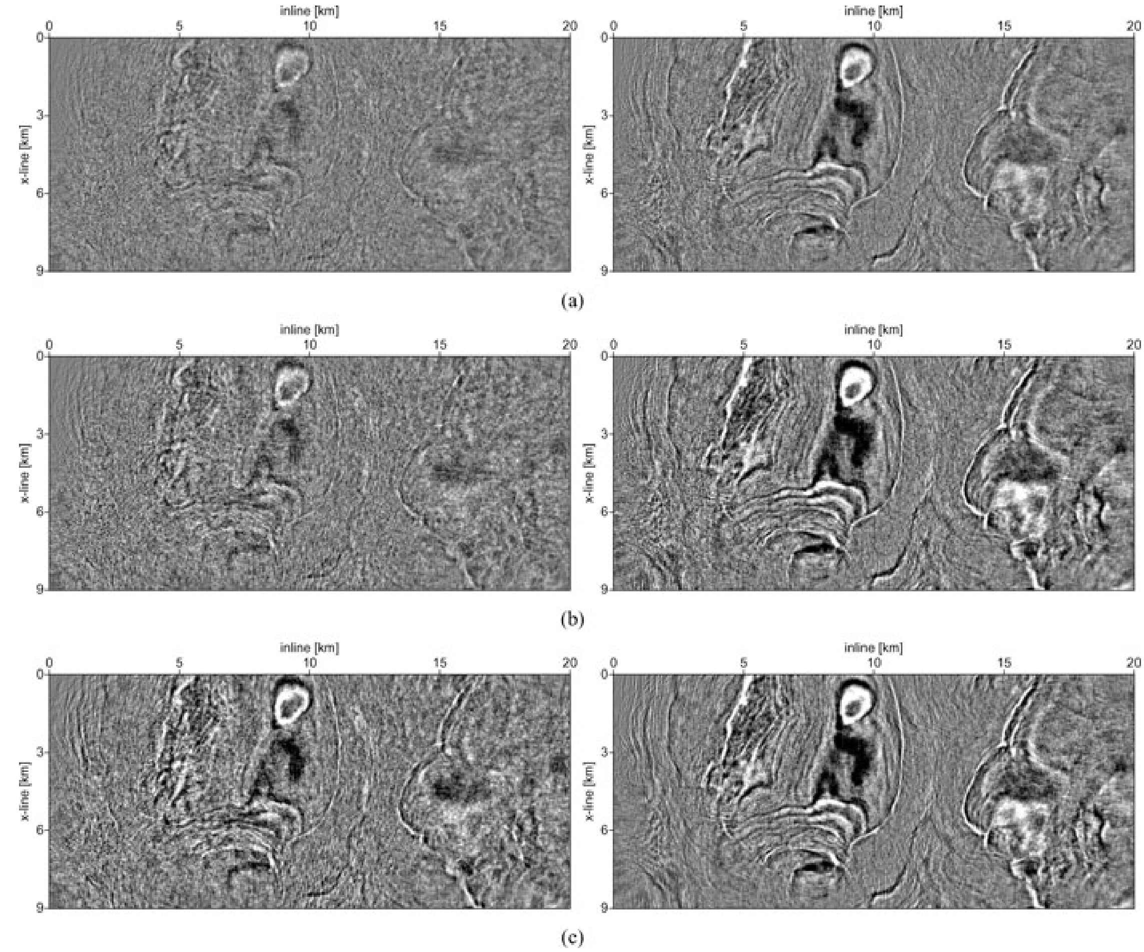

Figure 19 Marine data: time slices at 4.77 s of the two time-migrated common-offset classes 400 m (left) and 1500 m (right): a) original data; b) DMO-interpolated data; c) CRS-interpolated data.

and the OO scheme. This is confirmed by the difference section shown in Fig. 17(d). The major differences appear in regions where traces are missing in the data. Here, the OO interpolation result shows a better continuity which is certainly due to the use of several operators per target sample. Figure 17(e) shows the number of operators per target sample in the OO scheme.

CRS regularization for migration

In the following we demonstrate the impact of trace interpolation for migration. We now use the entire irregular marine single-azimuth 3D data set which also served to extract the common-offset class described in the preceding section. The data set forms a four-dimensional space (t, x, y, h), where t denotes time, h denotes the offset, and x, y denote the midpoint coordinates in inline and crossline, respectively. Irregularities appear in all spatial dimensions. The bin sizes are 12.5 m in inline and 25 m in crossline.

Although the CRS interpolation is possible for any dimension, our implementation is currently limited to three dimensions including time. Therefore, we choose to regularize the midpoint geometry in common-offset classes where we define a common-offset class by an offset bin of 100 m. In this manner, the data was subdivided into 40 common-offset classes in the offset range of 300–4200 m. Prior to the CRS interpolation, we applied an NMO correction to reduce the impact of the offset binning. An inverse NMO correction after the CRS-based regularization constructs the regularized data. For comparison with a standard procedure we also applied a DMO correction followed by an inverse DMO correction in order to regularize the data. Finally, we time migrated the common-offset classes of the original data set and the regularized data sets.

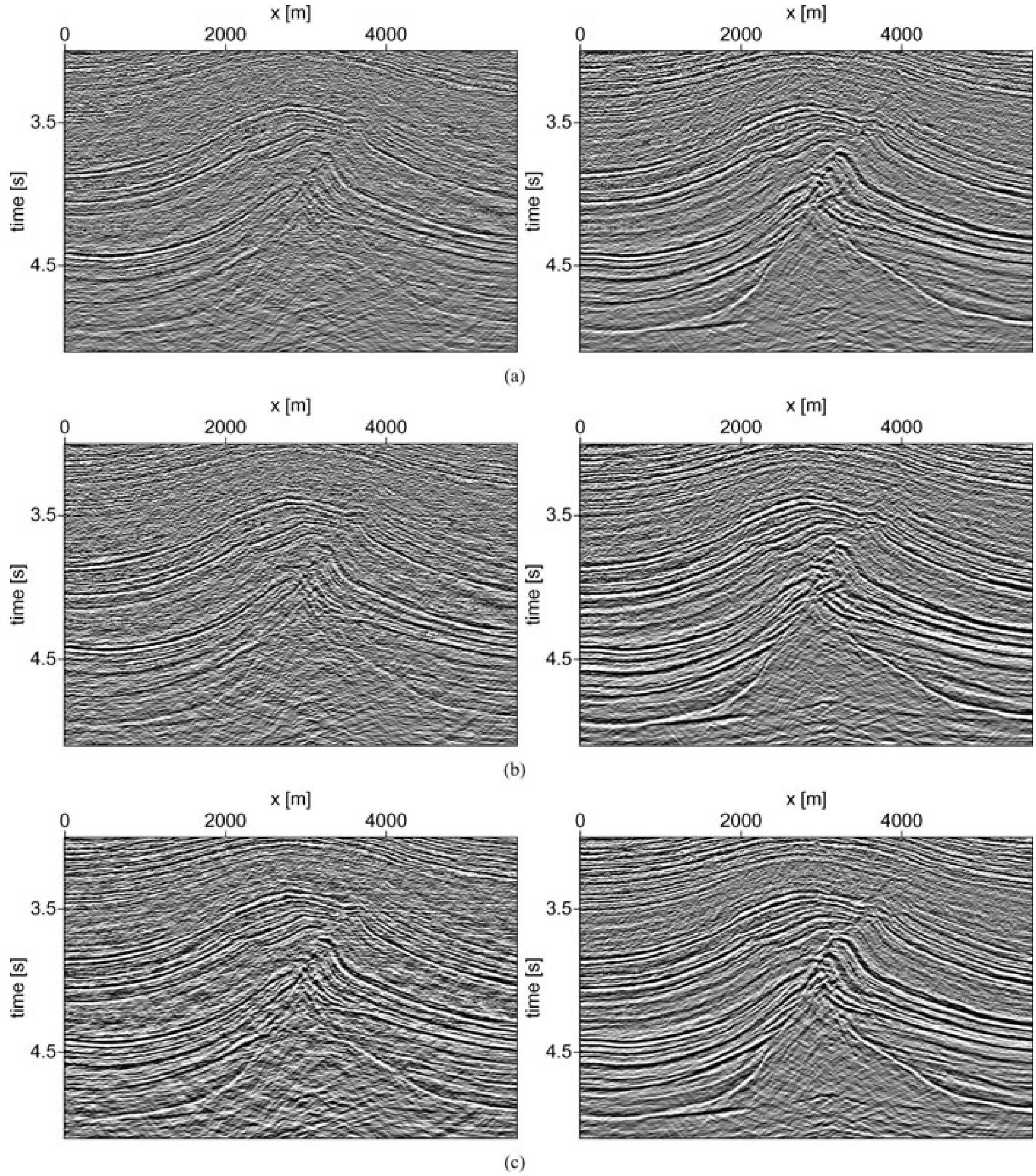

Figure 20 Marine data: subsets of an inline section from the time-migrated offset classes 400 m (left column) and 1500 m (right column): a) original data; b) DMO-interpolated data; c) CRS-interpolated data.

Figures 18 and 19 show two time slices of two time-migrated common-offset classes using the original data, the DMO-regularized data, and the CRS-regularized data. Although the used Kirchhoff-type migration does not require regular input data, the results clearly illustrate the advantage of regularization prior to time migration. The acquisition footprints that appear in the time slice $t = 2.2$ s for the time migration of a near offset class for the original data and that persist in the result from the DMO procedure have been successfully removed by the CRS interpolation. Considering an inline section and a crossline section (Figs 20 and 21) of these two time migrated common-offset classes, we observe a significant improvement in continuity and definition of the events in the time migrations of the CRS-regularized data.

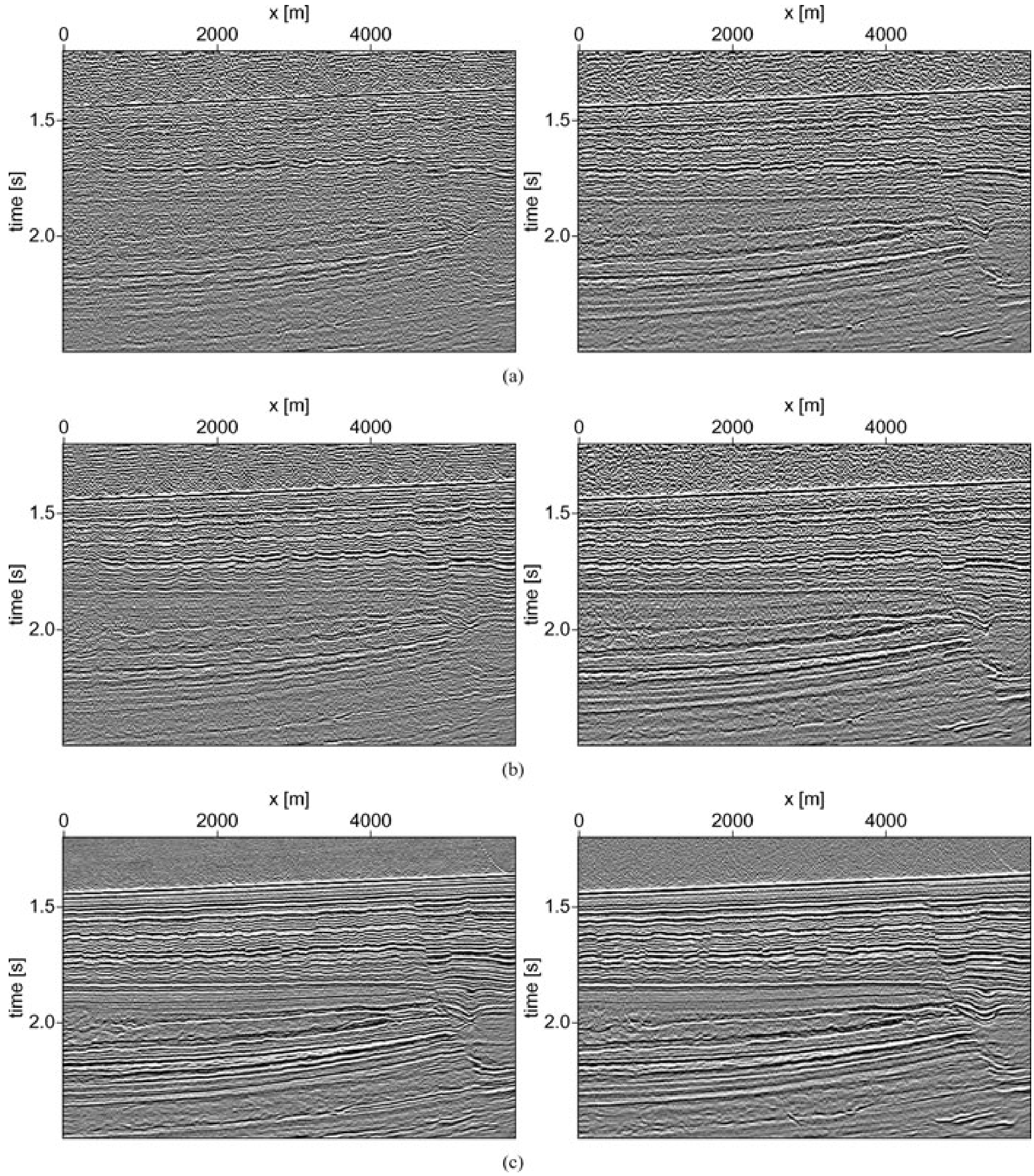

Figure 21 Marine data: subsets of a crossline section from the time-migrated offset classes 400 m (left column) and 1500 m (right column): a) original data; b) DMO-interpolated data; c) CRS-interpolated data.

Figure 22 shows a common image gather extracted from the time migrations of all 40 common-offset classes. Although the common-offset classes have been processed independently by the CRS interpolation and the time migration we also observe a better continuity and definition of the events in offset direction.

To produce the final time-migration result, we stacked the 40 time-migrated offset classes. Figures 23 and 24 show the time slices, and the inline and crossline sections of the stack. Here, the differences of the migrated results are less obvious. The stacking process significantly reduces the fluctuations present in the individual common-offset classes.

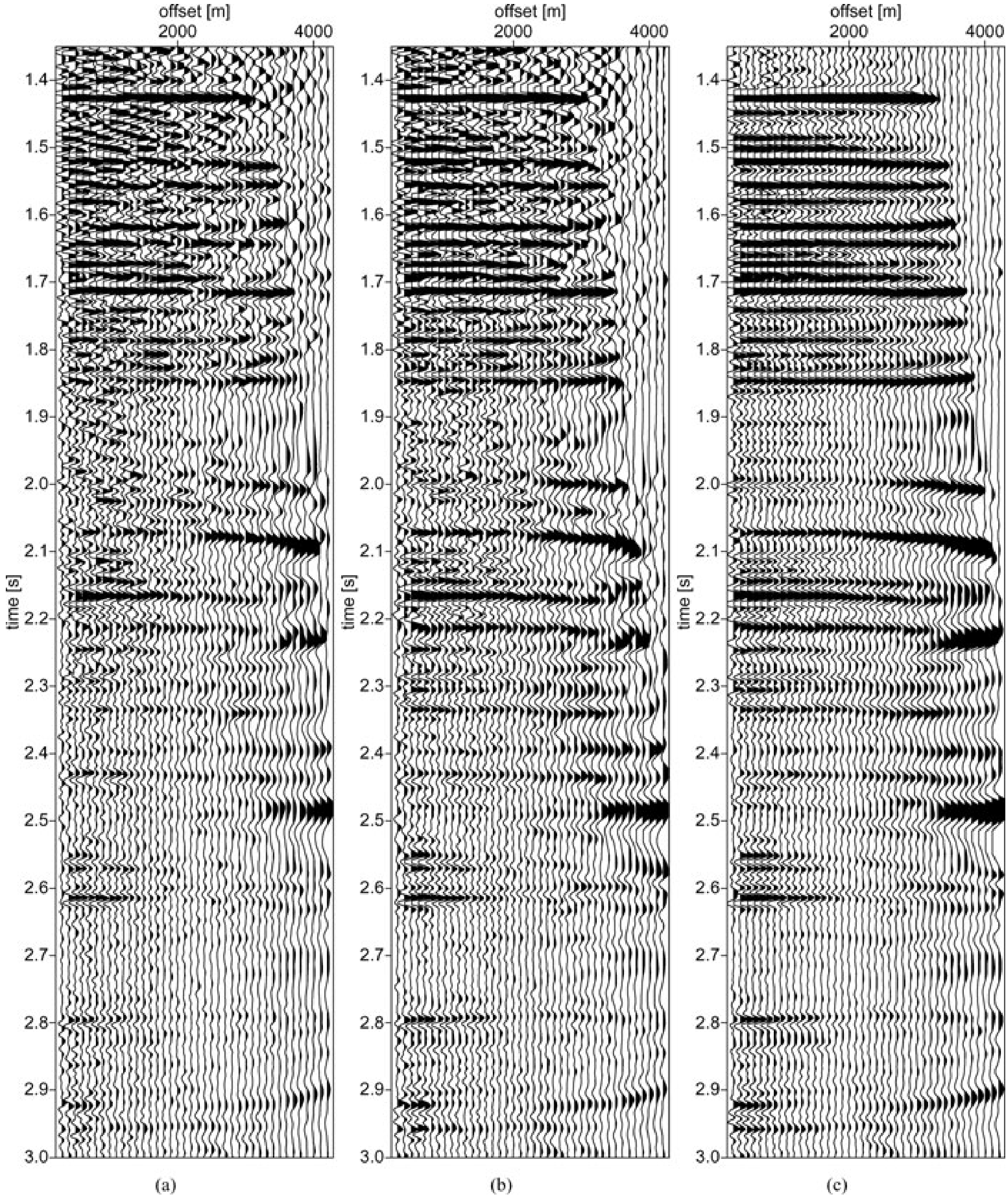

Figure 22 Marine data: common-image gathers extracted from the center of the time-migration results: a) original data; b) DMO-interpolated data; c) CRS-interpolated data.

However, we still observe a difference in terms of continuity as detected by an automatic picking of a horizon in the stacked time-migration results. The picked surfaces along a horizon in the three time-migration results are shown in Fig. 25 together with the picks in selected cross-line sections. The detected surface in the time-migrated data from DMO interpolation considerably extends the surface picked in the time-migrated original data. The time-migrated CRS interpolation result offers the most complete reconstruction of the horizon.

© 2009 European Association of Geoscientists & Engineers,

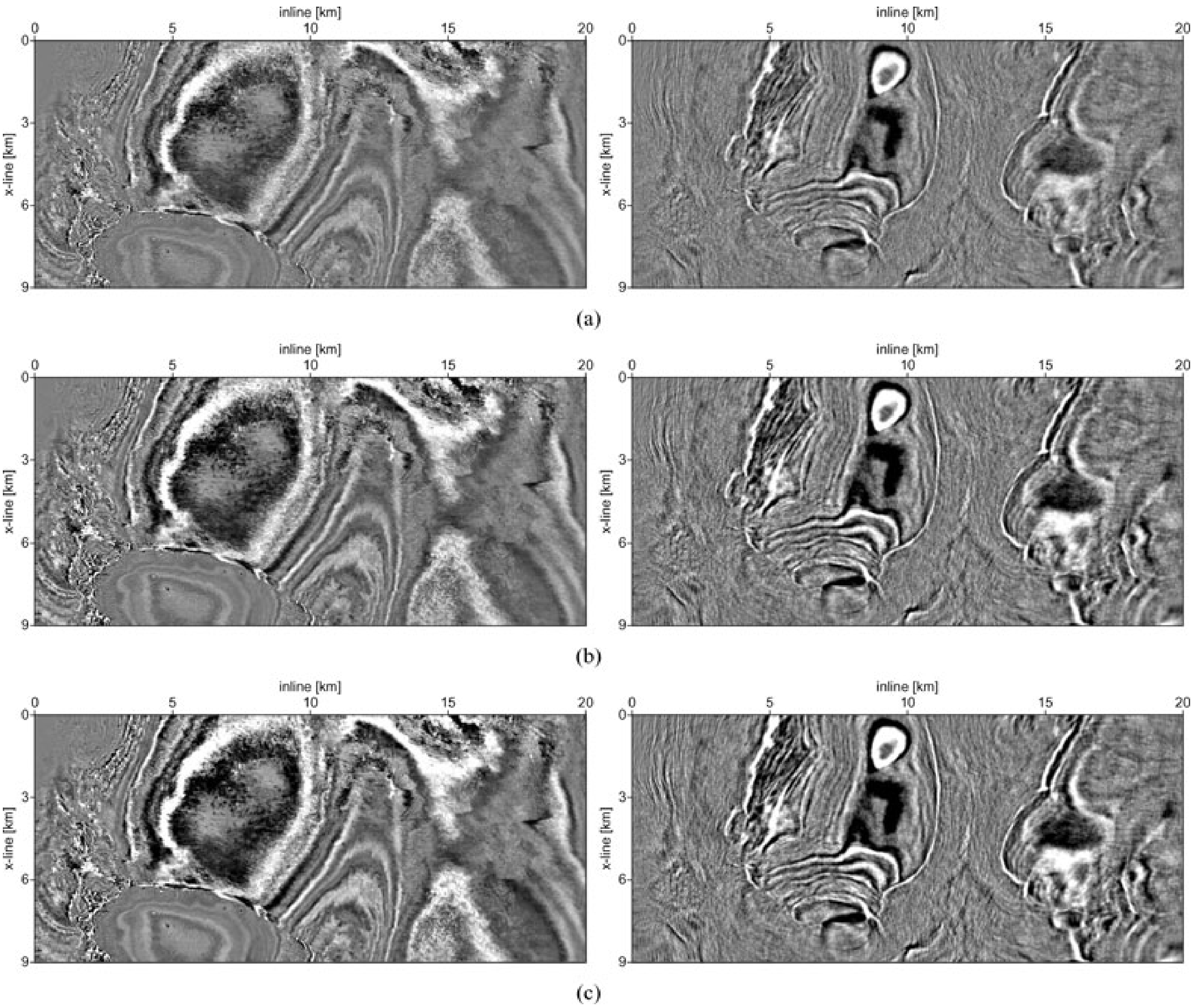

Figure 23 Marine data: time slices at 2.2 s (left) and 4.77 s (right) through the time-migration results stacked over all offsets: a) original data; b) DMO-interpolated data; c) CRS-interpolated data.

CONCLUSIONS

The presented CRS interpolation operates in the original prestack data domain and accounts for irregular geometries. A distinction to existing methods is the use of local operators of the second order which are less sensitive to aliasing but imply a considerable increase of the computational expense. As a consequence CRS interpolation is limited to operate in subsets of the prestack data.

For the CRS interpolation we introduced the operator-oriented scheme, which, in distinction to a classical target-oriented scheme, implicitly allows the contributions of several operators for a target sample. With respect to conflicting dip situations this adds information but does not solve them entirely. Nevertheless, the object-oriented scheme avoids an expensive multi-operator estimation as would be required in the target-oriented scheme for this purpose. Both schemes provide similar results, however, in areas of uncertainties in the parameter estimation the results from the operator-oriented scheme show a better continuity of the events and less noise. Additionally, the operator-oriented scheme is suited for an estimation of parameters on a coarse parameter grid which reduces the computational cost. The observed increase in stability and reliability as well as the significant gain in computation time make the operator-oriented scheme highly attractive.

We demonstrated the efficiency of a CRS interpolation on different types of real 3D data and showed the impact of regularization on a subsequent time-migration. The observed

© 2009 European Association of Geoscientists & Engineers,

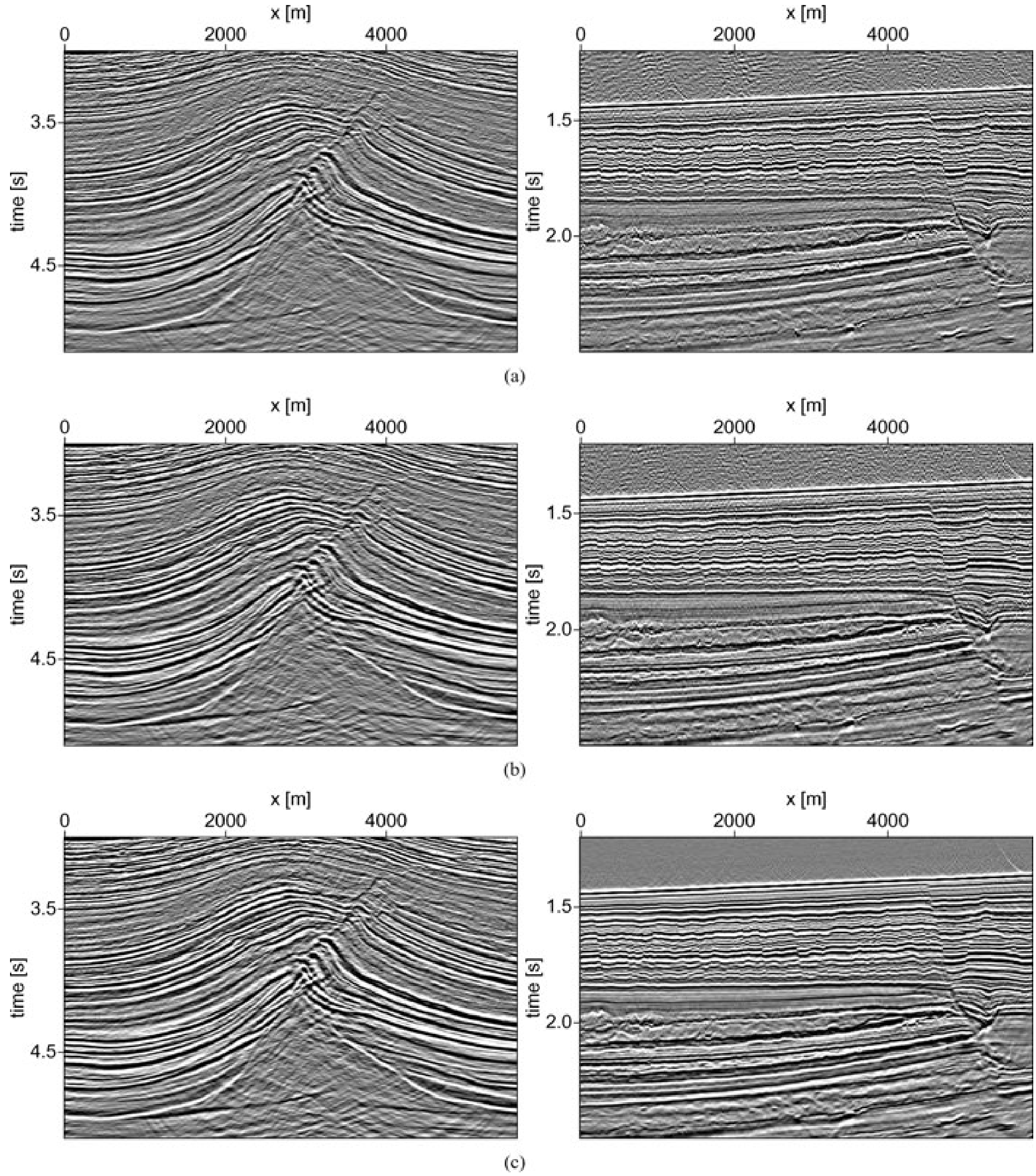

Figure 24 Marine data: subsets of an inline section (left) and a crossline section (right) of the time-migration results stacked over all offsets: a) original data; b) DMO-interpolated data; c) CRS-interpolated data.

improvements in continuity of the reflection events offer better working conditions for a residual moveout analysis in the migrated gathers as well as for automatic picking and interpretation of reflection events. In our opinion, the computational expense of a CRS interpolation is justified by the observed benefit of subsequent processing schemes.

ACKNOWLEDGEMENTS

The authors would like to thank Total for supporting this research. Amongst others, we would like to thank particularly Reda Baina from OPERA, Bertrand Duquet, Ehsan Sadeghi, and Jean-Luc Boelle from Total Pau for fruitful discussions and their active participation in the tests and

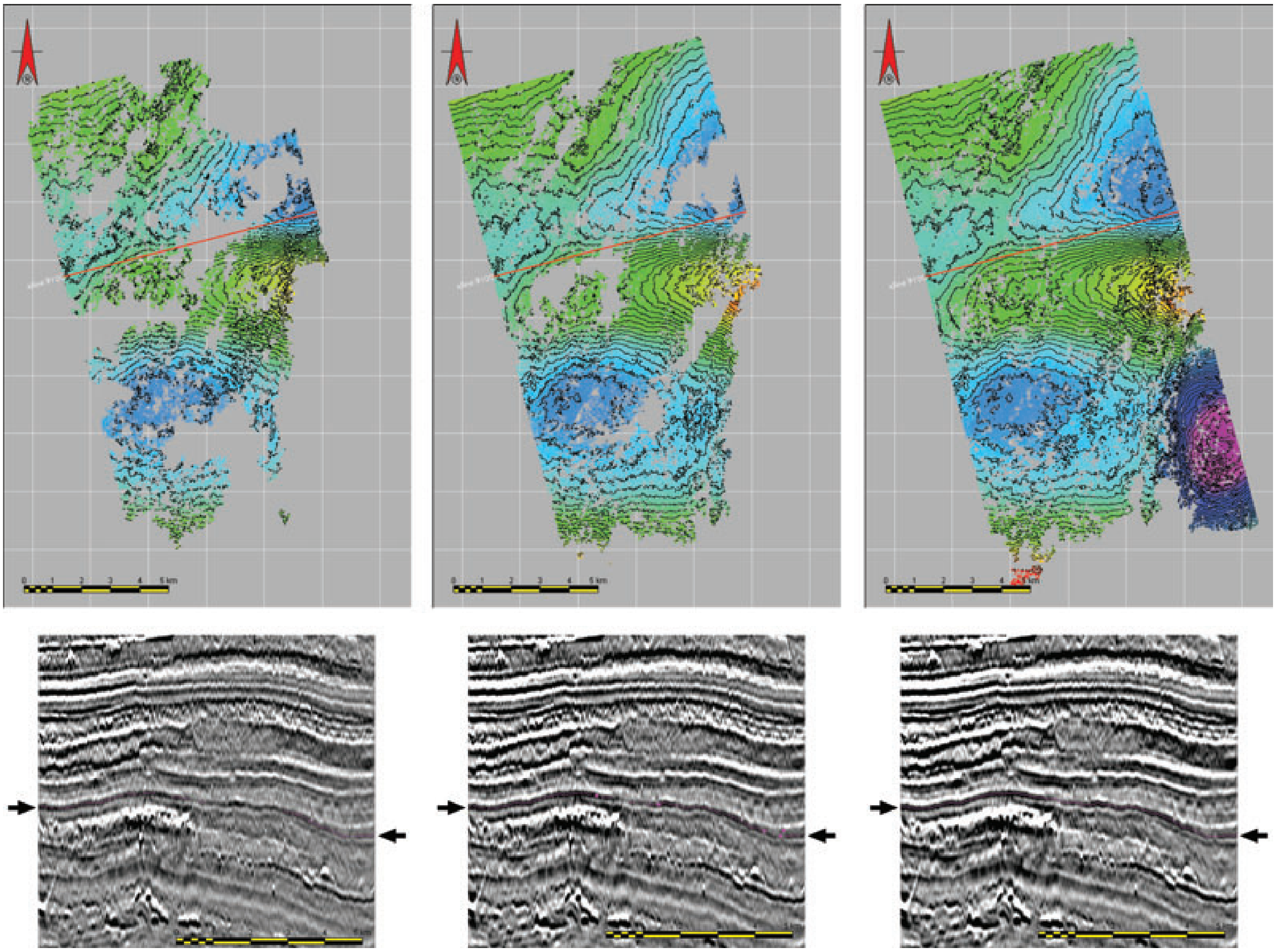

Figure 25 Marine data: automatic picking of a horizon in the stacked time-migration results of the original data (left), DMO-interpolated data (middle), and CRS-interpolated data (right). The detected surfaces are displayed in the top row together with a selected crossline shown in red; the detected part within the indicated crossline section is illustrated by the magenta curve in the bottom row.

comparisons. Finally, we would like to thank the reviewers for their constructive criticism, in particular Juergen Mann from the Geophysical Institute in Karlsruhe who spared no effort to improve the readability.

OPERA is a private organization funded by Total and supported by Pau University whose main objective is to carry out applied research in petroleum geophysics.

REFERENCES

Della Moretta D., Kluever T. and Marchetti P. 2006. 3D CRS-based velocity model building - an accurate and cost-effective approach. 68th EAGE meeting, Vienna, Austria, Extended Abstracts, P155.

Duveneck E. 2004. Velocity model estimation with data-derived wavefront attributes. *Geophysics* **69,** 265–274.

Hoecht G., Landa E. and Baina R. 2004. Seimic data interpolation using local wavefield characteristics. 66th EAGE meeting, Paris, France, Extended Abstracts, D031.

Hoecht G. and Ricarte P. 2006a. Analysis of the common-reflection surface interpolation. 68th EAGE meeting, Vienna, Austria, Extended Abstracts, G029.

Hoecht G. and Ricarte P. 2006b. Parameter-oriented CRS imaging. 76th SEG meeting, New Orleans, Lousisna, USA, Expanded Abstracts, 2966–2970.

Jäger R., Mann J., Höcht G. and Hubral P. 2001. Common-reflection-surface stack: image and attributes. *Geophysics* **66,** 97–109.

Kao C.-N. 1997. A trace interpolation method for spatially aliased and irregularly spaced seismic data. 67th SEG meeting, Dallas, Texas, USA, Expanded Abstracts, 1108–1110.

Hugonnet P. and Canadas G. 1997. Regridding of irregular data using 3-d radon decompositions. 67th SEG meeting, Dallas, Texas, USA, Expanded Abstracts, 1111–1114.

Sacchi M.D. and Ulrych T.J. 1996. Estimation of the discrete Fourier transform, a linear inversion approach. *Geophysics* **61,** 1128–1136.

© 2009 European Association of Geoscientists & Engineers, *Geophysical Prospecting*, **57**, 957–979

Spitz S. 1991. Seismic trace interpolation in the f-x domain. *Geophysics* **56**, 785–794.

Thorson J.R. and Claerbout J.F. 1985. Velocity stack and slant stochastic inversion. *Geophysics* **50**, 2727–2741.

Trad D. 2003. Interpolation and multiple attenuation with migration operators. *Geophysics* **68**, 2043–2054.

Xu S., Zhang Y., Pham D. and Lambaré G. 2005. Antileakage fourier transform for seismic data regularization. *Geophysics* **70**, V87–V95.

Zhang Y., Bergler S. and Hubral P. 2001. Common-reflection-surface (CRS) stack for common-offset. *Geophysical Prospecting* **49**, 709–718.